Florida State University Libraries

2018

Numerical Mass Estimates from Correlation Functions in a 4D SU(2) Higgs Model

Leon Hostetler

THE FLORIDA STATE UNIVERSITY

COLLEGE OF ARTS & SCIENCES

NUMERICAL MASS ESTIMATES FROM CORRELATION FUNCTIONS

IN A 4D SU(2) HIGGS MODEL

By

LEON HOSTETLER

A Thesis submitted to the
Department of Physics
in partial fulfillment of the requirements for graduation with
Honors in the Major

Degree Awarded:
Spring, 2018

The members of the Defense Committee approve the thesis of Leon Hostetler defended on January 24, 2018.

_____

Professor Bernd Berg
Thesis Director

_____

Professor Takemichi Okui
Committee Member

_____

Professor Mark Sussman
Outside Committee Member

Abstract

In lattice gauge theory one estimates masses from correlation functions in Euclidean time to which superselection rules may apply. The correlation functions are a superposition of exponential functions of the energy levels, and the mass to be estimated is that associated with the ground state in our investigation. We discuss and implement three such estimators. The first is obtained by taking the logarithm of the ratios of consecutive values of the correlation function and estimating the asymptotic value. Another estimator involves fitting a 2-parameter exponential function to the correlation function and trying to eliminate higher mass contributions. The third estimator involves fitting a 4-parameter function of the sum of two exponentials to the correlation function. Various features and quirks of the different estimators are described. A comparison of the three estimators shows consistency indicating that all three are reliable methods, supplementing one another, for numerically estimating masses from correlation functions.

Contents

1 Introduction

The Standard Model of particle physics is a SU(3) × SU(2) × U(1) gauge quantum field theory that describes the electroweak and strong interactions and classifies the known elementary particles. The fundamental objects of the Standard Model are quantum fields including fermion fields ψ, the electroweak boson fields W_1, W_2, W_3, and B, the gluon field, and the Higgs field ϕ.

When the coupling of a gauge theory is small enough, interesting quantities can be computed perturbatively and lead to the most precise tests of the theory. However, there are many questions which can only be answered non-perturbatively. Lattice gauge theory (LGT) is a non-perturbative approach that can help us answer these questions.

In LGT, the four-dimensional Minkowski spacetime of quantum field theories is Wick rotated to become a four-dimensional Euclidean spacetime on a finite, discrete, hypercubic lattice. Such a lattice is defined by *sites* separated by distance a and connected by *links*. Fermion and Higgs fields are defined at the lattice sites and gauge fields on the lattice links. The action in LGT is constructed so that gauge invariance is preserved on the lattice and the continuum action is reproduced when the lattice spacing a is taken to zero.

Quantities such as particle masses are calculated stochastically in LGT using Markov Chain Monte Carlo (MCMC) methods in computer simulations. Such simulations are often repeated at many couplings with lattices of different sizes, so that the quantities of interest can be extrapolated to the infinite volume limit. The true continuum limit is obtained by driving the couplings of the theory to their critical values. What is often done in practice is to look at the limit $a\,m \to 0$, where a is the lattice spacing and m sets the physical mass scale. For example, m may be the mass of the ground state. LGT calculations can be extremely resource intensive and even when employing parallel computation with a number of processors, a typical simulation to generate a single data point might take a week on a typical university computing cluster.

This thesis is a small part of larger projects being undertaken by the LGT group at Florida State University (FSU). LGT is used to numerically estimate the Higgs and W masses, m_H and m_W, using correlation functions. With the mass ratio $m_H/m_W = 1.6$ held constant near the known [1] experimental value, we are searching for numerical evidence in favor or against continuum limit behavior in the SU(2) Higgs model. Throughout this process, the accuracy of mass estimates is of particular interest. In this thesis, we examine different methods for estimating masses. We are primarily concerned with the accuracy of mass estimates in general and of the ratio m_H/m_W in particular.

2 Lattice Gauge Theory

In quantum field theory (QFT), the gauge field Lagrangian can be written as

$$\mathcal{L}_G = \frac{1}{4} F_{\mu\nu}^a F_{\mu\nu}^a,$$

where the field strength tensor is

$$F_{\mu\nu}^a = \partial_\mu A_\nu^a - \partial_\nu A_\mu^a + g f^{abc} A_\mu^b A_\nu^c.$$

Here, g is the coupling constant, $A_\mu = -ig A_\mu^a T^a$ is the gauge field, T^a with $a = 1, 2, \ldots N^2 - 1$ are the generators of the $SU(N)$ Lie algebra, and f^{abc} are the real structure constants of $SU(N)$. The gauge action is then simply

$$S_G = \int d^4x \, \mathcal{L}_G. \tag{1}$$

For the Higgs field, the Lagrangian is [13]

$$\mathcal{L}_H = \left(D_\mu \Phi\right)^\dagger D_\mu \Phi + m_0^2 \Phi^\dagger \Phi + \lambda_0 \left(\Phi^\dagger \Phi\right)^2,$$

where $\Phi = (\Phi_u, \Phi_d)^T$ is the complex Higgs doublet, and the covariant derivative D_μ is

$$D_\mu = \partial_\mu - \frac{ig_0}{2} B_\mu - \frac{ig_0'}{2} W_\mu^k \tau_k.$$

Here, B_μ and W_μ^k are the $U(1) \times SU(2)$ electroweak gauge fields. The Higgs action is then

$$S_H = \int d^4x \, \mathcal{L}_H. \tag{2}$$

2.1 SU(2) Lattice Gauge Theory with Higgs

By performing a Wick rotation, which involves replacing t with $it \equiv \tau$, we can relate a field theory in four-dimensional Minkowski space to one in four-dimensional Euclidean space. This relationship was extensively studied by Osterwalder and Schrader [10]. In 1974, Wilson [14] introduced a formulation of quantum chromodynamics on a four-dimensional lattice that preserves gauge invariance. On such a lattice, the formerly intractable infinite-dimensional path integrals of QFT become finite-dimensional and can be evaluated using MCMC simulations.

In LGT, we start by replacing continuous 4D spacetime with a 4D finite lattice

$$x \to an,$$

where a is the lattice spacing, and n with integer components $n_x, n_y, n_z = 1, 2, \ldots, N$, and $n_t = 1, 2, \ldots, N_t$ labels the lattice sites. To maintain gauge invariance of the

2

action, Wilson introduced a field $U_\mu(x)$ with a directional index μ. Commonly called "link variables", the matrices $U_\mu(x)$ are oriented and attached to the links between lattice sites. The trace over a closed loop of link variables is gauge invariant. For the gauge action it is sufficient to use the smallest closed loop, called a "plaquette", on the lattice. The product of the link variables defining a plaquette is denoted $U_\square$. The Wilson gauge action is the sum over all positively oriented plaquettes

$$S_{G,latt} = \beta \sum_\square \left(1 - \frac{1}{N}\text{Tr}\left[U_\square\right]\right), \qquad \beta = \frac{2N}{g^2},$$

where g is the bare coupling constant, and $N = 2$ in this thesis. It can be verified that in the classical continuum limit $a \to 0$, the Wilson action becomes the continuum action of Eq. (1). Textbooks can be consulted for the derivation [9, 4]. The lattice Higgs action, is

$$S_{H,latt} = \sum_x \left(\lambda \left(\Phi^\dagger(x)\Phi(x) - 1\right)^2 + \Phi^\dagger(x)\Phi(x) - \kappa \sum_\mu \Phi^\dagger(x + \hat\mu)U_\mu(x)\Phi(x) \right),$$

where κ is called the *hopping parameter*. By writing $\Phi(x) = \rho(x)\alpha(x)$ and introducing the gauge invariant link variable $V_\mu(x) \equiv \alpha^\dagger(x + \hat\mu)U_\mu(x)\alpha(x)$ and then taking the limit $\lambda \to \infty$, the action $S = S_{G,latt} + S_{H,latt}$ simplifies to

$$S = \beta \sum_\square \left(1 - \frac{1}{2}\text{Tr}\left[V_\square\right]\right) - \kappa \sum_{x,\mu} \text{Tr}\left[V_\mu(x)\right]. \qquad (3)$$

We shall limit our investigation to the $\lambda \to \infty$ limit, because exploring the full parameter space would not be possible in the time at our disposal.

To extract masses, we follow Langguth, Montvay, and Weisz [6] and measure correlation functions of the quantities

$$h \equiv \text{Tr}\left[V_\mu(x)\right], \qquad \text{and} \qquad w_{r\mu} \equiv \text{Tr}\left[\tau_r V_\mu(x)\right].$$

For example, we define the operator

$$\tilde h(\vec{p}, n_t) = \sum_{\vec{x}} e^{i\vec{p}\cdot\vec{x}}\, h(\vec{x}, n_t),$$

where

$$p_i = \frac{2\pi n_i}{N}, \quad n_i = 0, 1, \ldots, N-1,$$

and where $i = 1, 2, 3$ and N^3 is the spatial volume of the lattice. For our numerical calculation of the masses, the operator is projected to zero momentum, $\vec{p} = \vec{0}$, then the corresponding Euclidean correlation function is

$$C(n_t) = \langle \tilde h(\vec{0}, n_t)\overline{h}(\vec{0}, 0)\rangle = \sum_k \langle 0|\hat h|k\rangle \langle k|\hat h^\dagger|0\rangle\, e^{-n_t E_k}.$$

3

2.2 Triviality

In the standard model, the Higgs field causes spontaneous symmetry breaking that triggers the Higgs mechanism giving mass to the gauge bosons. By construction, this arises from the quartic self-coupling of the Higgs field. However, in the continuum limit, the renormalized coupling seems to be driven to zero. That is, the Higgs field appears to be trivial. This is the problem of *triviality*.

In 1974, Wilson [15] showed that a scalar Higgs model is trivial for dimensions higher than four. In 1981, Aizenman [2] proved this rigorously. Strong evidence of triviality for the most interesting case, i.e., four dimensions, has been shown analytically [12] and by lattice simulations [16].

Earlier work on triviality was performed primarily to get upper bounds on the Higgs mass [5, 13]. Now that a light Higgs has been discovered [1], there is understandably no longer much interest in upper mass bounds, which become shifted all the way beyond the Planck mass scale. Therefore, one may expect continuum limit behavior in the range of coupling constants accessible to our simulations. One may call this a "pseudo" continuum limit, because it breaks down eventually at an incredibly large mass scale. However, this argument assumes that the SU(2) gauge interaction is negligible due to its asymptotic freedom. The ultimate aim of the project is to investigate whether this assumption is justified.

2.3 Mass Estimates

For instance, in the textbook by Gattringer and Lang [4] a Euclidean correlation function of the form

$$C(n_t) = \sum_k \langle 0|\hat{O}|k \rangle \, \langle k|\hat{O}^\dagger|0 \rangle \, e^{-n_t E_k}, \tag{4}$$

is derived. This shows that our correlation function is a sum of exponential functions

$$C(n_t) = A_0 e^{-n_t E_0} + A_1 e^{-n_t E_1} + A_2 e^{-n_t E_2} + \cdots .$$

We are using n_t as the time variable to emphasize that the variable takes discrete values when we are on the lattice, using lattice units $a = 1$. To revert to normal units, one of the energies or masses has to be used to set the scale.

In units where $c = 1$, the energy of a particle with rest mass m_0 as a function of momentum is

$$E(p) = \sqrt{m_0^2 + p^2}.$$

For momentum $p = 0$, we have that $E = m_0$, so that the leading contribution to the correlation function Eq. (4) comes from the lowest mass. For sufficiently large n_t the first exponential term dominates, and we have

$$C(n_t) \simeq A_0 e^{-m_0 n_t}, \tag{5}$$

where m_0 is the rest mass of the particle being estimated. To check for consistency or obtain a better fit we include the second exponential term

$$C(n_t) \simeq A_0 e^{-m_0 n_t} + A_1 e^{-m_1 n_t},$$

and perform a four parameter fit with the parameters A_0, m_0, A_1, and m_1. In that case, the parameter of primary interest is still m_0—the mass associated with the ground state energy.

3   MCMC Simulations and Statistical Analysis

3.1   Gaussian Difference Test

In this thesis, different mass estimators will be compared. Given two different estimates of a mass and their error bars, how does one determine if the difference between the estimates is due to chance or due to a real difference between the estimators? In the textbook [3], the *Gaussian difference test* is derived to help answer this question.

Given two different estimates of some mean $\overline{x}$ and $\overline{y}$ with difference

$$D = \overline{x} - \overline{y},$$

and their error bars $\sigma_{\overline{x}}$ and $\sigma_{\overline{y}}$, then the random variable

$$\frac{D^r}{\sigma_D}, \qquad \text{where } \sigma_D = \sqrt{\sigma_{\overline{x}}^2 + \sigma_{\overline{y}}^2},$$

is normally distributed with expectation zero and variance one. The superscript "r" is used to emphasize that D^r is a random variable. Then the Gaussian distribution implies the probability

$$P\left(\left|\frac{D^r}{\sigma_D}\right| \leq \frac{D}{\sigma_D}\right) = \text{erf}\left(\frac{|D|}{\sqrt{2}\sigma_D}\right) = \text{erf}\left(\frac{|\overline{x} - \overline{y}|}{\sqrt{2}\sqrt{\sigma_{\overline{x}}^2 + \sigma_{\overline{y}}^2}}\right),$$

where $\text{erf}(x)$ is the Gaussian error function. The probability that the measured difference $|\overline{x} - \overline{y}|$ is due to chance is then

$$Q = 1 - P = 1 - \text{erf}\left(\frac{|\overline{x} - \overline{y}|}{\sqrt{2}\sqrt{\sigma_{\overline{x}}^2 + \sigma_{\overline{y}}^2}}\right). \tag{6}$$

If Q is large (e.g. $Q > 0.05$), we conclude that the difference between the estimates is most likely due to chance. If Q is small, then the difference $|\overline{x} - \overline{y}|$ is statistically significant, and the two estimators are probably measuring different things.

3.2 Curve Fitting

Given N data points $y_i(x_i)$ with $i = 1, 2, \ldots, N$, with statistical error bars σ_i on the y_i, we often model the data by fitting it to some function with free parameters. The goal is then to estimate the parameters and their error bars. For example, if the data appears linear, one might model it with a function of the form $y = a_1 x + a_2$. Here, $\vec{a} = (a_1, a_2)$ are the free parameters.

The foundation of most fitting methods is the chi-squared function defined to be

$$\chi^2(\vec{a}) = \sum_{i=1}^{N} \left(\frac{y_i - y(x_i; \vec{a})}{\sigma_i} \right)^2. \tag{7}$$

Here, y_i are the data points with statistical errors σ_i, and $y(x_i; \vec{a})$ is the function we are fitting. The components of $\vec{a} = (a_1, \ldots, a_M)$ are the free parameters to be estimated. The best estimates of the free parameters occur when χ^2 is at a minimum. The task of fitting a model function to a set of data is then reduced to the problem of minimizing χ^2 by trying different possibilities for $a_1, \ldots, a_M$. Statistical error bars for the parameters are obtained from the diagonal elements of the covariance matrix.

There are well-known methods for linear and polynomial fitting. For such fits, the minimization of χ^2 is straightforward. In our case, however, we will generally be fitting to nonlinear exponential functions. For that, we use the Levenberg-Marquardt algorithm proposed by Levenberg [7] and improved by Marquardt [8].

The Levenberg-Marquardt algorithm uses a weighted average of the Newton-Raphson and the Steepest Descent methods for minimizing χ^2. All three are iterative methods that begin with some initial guess, $\vec{a}_1$, for the free parameters. The Steepest Descent method computes the next iteration point, $\vec{a}_{n+1}$, from

$$\vec{a}_{n+1} = \vec{a}_n - \gamma \nabla \chi^2(\vec{a}_n),$$

where γ is a small constant. In the Newton-Raphson method, the next iteration point is determined from

$$\vec{a}_{n+1} = \vec{a}_n - H^{-1} \nabla \chi^2(\vec{a}_n),$$

where H is the $M \times M$ Hessian matrix of χ^2 with components

$$H_{jk} = 2 \sum_{i=1}^{N} \frac{1}{\sigma_i^2} \left[\frac{\partial y(x_i; \vec{a})}{\partial a_j} \frac{\partial y(x_i; \vec{a})}{\partial a_k} - [y_i - y(x_i; \vec{a})] \frac{\partial^2 y(x_i; \vec{a})}{\partial a_j \partial a_k} \right] \Bigg|_{\vec{a} = \vec{a}_n}.$$

The advantage of the Steepest Descent method is convergence even given a poor initial approximation. The disadvantage is slow convergence. The Newton-Raphson method converges rapidly, but needs a good initial approximation. The Levenberg-Marquardt method combines the two using a weighted average. Initially, the weight is biased toward the Steepest Descent method ensuring convergence, at least toward a local

6

minimum. Once convergence is detected, the weight is shifted to the speedier Newton-Raphson method. A detailed description of the Levenberg-Marquardt algorithm and its application can be found in [3].

As one measure of the quality of a fit, we look at the goodness-of-fit defined in [11] as

$$q = 1 - P\left(\frac{\nu}{2}, \frac{\chi^2}{2}\right),\tag{8}$$

where $P(a, x)$ is the incomplete gamma function. Here, χ^2 defined in Eq. (7), is of the fit parameters, and ν is the number of degrees of freedom calculated as the number of points being fitted minus the number of fitting parameters. The goodness-of-fit q-value gives the probability that the observed chi-square will exceed χ^2 by chance even for a correct model. In other words, it gives the likelihood that the difference between the fit and the data is due to chance. A high q-value, e.g. $q > 0.05$, suggests that the fitting model is correct. The goodness-of-fit (lowercase q), which gives the likelihood that the difference between a curve fit and the data is due to chance, should not be confused with the Gaussian difference (uppercase Q) described in section (3.1), which gives the likelihood that the observed difference between two means is due to chance.

3.3   Jackknife Binning

We use the output from MCMC simulations performed on multiple processor clusters. The design of the simulations required only simple modifications from those described by Berg [3]. As is common with LGT simulations that aim at estimating non-linear functions of the generated data, jackknife binning is performed to suppress the bias and to obtain estimates of the error.

Given data x_i with $i = 1, 2, \ldots, N$, we use the unbiased estimator

$$\overline{x} = \frac{1}{N}\sum_{i=1}^{N} x_i,$$

of the expectation value $\widehat{x} = \langle x_i \rangle$. We often want to estimate some non-linear function $\widehat{f} = f(\widehat{x})$ using the estimator $\overline{f} = f(\overline{x})$. However, for many such functions, calculating the uncertainty using error propagation formulas is neither practical nor reliable. Alternatively, jackknife binning is easier and more robust. With this method, we construct N jackknife bin subsets $\{x_n^J\}$ ($J = 1, \ldots, N$) of our data by removing the Jth entry of the original set. Then

$$\sigma_{\overline{f}}^2 = \frac{N-1}{N}\sum_{J=1}^{N}\left(f^J - \overline{f}\right)^2,$$

gives the variance of $\overline{f}$. Here, $\overline{f}$ is the value of the estimator computed for the original set, and f^J gives the estimator for the Jth jackknife bin. The square root of the variance is taken to estimate the uncertainty of $\widehat{f}$.

The bias of the estimator is given by

$$\text{bias}\left(\overline{f}\right) = (N-1)\left(\overline{f}^J - \overline{f}\right),$$

where $\overline{f}^J$ is the mean of the estimates f^J. The bias corrected estimator is then

$$\overline{f}^c = \overline{f} - (N-1)\left(\overline{f}^J - \overline{f}\right).$$

To estimate the statistical uncertainty of the bias corrected estimator, one can perform second level jackknife binning. One constructs $N(N-1)$ subsets of our original data set, essentially by doing a jackknife binning of each of our first level jackknife bins. Second level jackknife binning is only necessary when the bias is found to be large and correction becomes necessary.

3.4 Mass Estimators

For a typical simulation, e.g., $8^3 \times 64$ or $12^3 \times 64$ with some specified β and κ, the output of the MCMC simulation is a number of data files containing jackknife bins of the correlation functions for the W mass and Higgs mass. From correlations in the long direction, we estimate m_W and m_H using several different estimators.

3.4.1 Ratio Fit

In practice, we compute correlation functions of Euclidean time *differences* $z = \Delta t$. For example, $C(z = 1)$ is the average value that the correlation function gives for all pairs of time points separated by a distance of 1. For the subsequent estimate of masses, jackknife bins of $C(z)$ are calculated, so that the mass estimators come in jackknife bins.

One way to estimate m_0 is to start by looking at the ratio of consecutive values of the correlation function

$$\frac{C(z)}{C(z+1)} = \frac{A_1 e^{-m_0 z} + A_2 e^{-m_1 z} + A_3 e^{-m_2 z} + \cdots}{A_1 e^{-m_0(z+1)} + A_2 e^{-m_1(z+1)} + A_3 e^{-m_2(z+1)} + \cdots}.$$

For large z,

$$\frac{C(z)}{C(z+1)} \simeq \frac{A e^{-m_0 z}}{A e^{-m_0(z+1)}} = e^{m_0}.$$

Taking the natural logarithm of both sides gives us

$$m(z) = \ln\left(\frac{C(z)}{C(z+1)}\right), \tag{9}$$
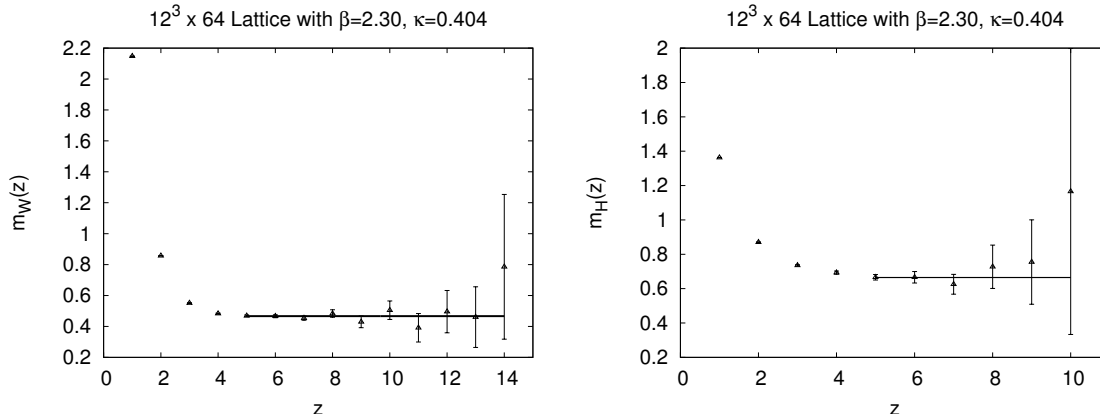
Figure 1: An example of the ratio fit. Here we plot $m(z)$ from Eq. (9) for the W mass (on the left) and the Higgs mass (on the right). The asymptotic value $m(z) \to m_0$ is estimated by applying a horizontal fit after excluding some of the initial points.

where $m(z) \to m_0$ as $z \to \infty$. Asymptotically, this logarithm approaches our mass m_0. Since $m(z) > m_0$, our mass estimate here is an upper bound.

One does not have to use the ratio of $C(z)$ to $C(z+1)$. In fact, the mass could also be estimated using, for example,

$$m_0 \simeq \frac{1}{3} \ln \left(\frac{C(z)}{C(z+3)} \right).$$

This estimator converges to the asymptotic value faster than if the ratio $C(z)$ to $C(z+1)$ is used. However, with the $C(z+3)$ in the denominator comes larger statistical error, so there is a tradeoff. Comparing the estimates of m_0 from multiple such versions of the ratio fit may be used to gauge systematic uncertainty in the estimates.

In this thesis, mass estimators are compared using mass estimates from $12^3 \times 64$ lattice simulations. The time extension of these lattices is $N_t = 64$. The correlation functions $C(z)$ are of the time differences $z = \Delta t$, so given the perdiodic boundary conditions, $1 \leq z \leq 32$. The ratio fit used in this thesis is of the form Eq. (9). For large z, the statistical error of the correlation function $C(z)$ rapidly becomes large. Hence, the error bars for Eq. (9) become large. Beyond some z', the error bars become so large that we lose nothing by discarding all points with $z > z'$. When the error bars become large, $C(z)$ begins to fluctuate and a convenient cut off point is the smallest z' for which $C(z')/C(z'+1) < 1$. When the cutoff point is reached, we automatically discard points with $z > z'$.

Fig. (1) illustrates a typical ratio fit of the W mass in the left panel and the Higgs mass in the right panel. In this example, the simulation was on a $12^3 \times 64$ lattice with $\beta = 2.30$ and $\kappa = 0.404$. For the W mass, points with $z > 14$ are discarded as described in the previous paragraph. To obtain the asymptotic value, a horizontal

line is fitted to Eq. (9) using the Levenberg-Marquardt algorithm. The uncertainty of the mass estimate is obtained using the jackknife method. Since the mass is estimated from the asymptotic value of Eq. (9), some initial points must be discarded. In this example, the first four points are discarded and the horizontal fit is applied in the interval $5 \leq z \leq 14$.

Several criteria are used to determine the best fit interval. One is to optimize the goodness-of-fit[1] q given by Eq. (8). The second is to minimize the calculated mass. The ratio fit gives an upper bound on the mass, so minimizing the measured mass gives us a least upper bound. For this example, different proposed fits are tabulated in Table (1). We see that the goodness-of-fit is optimized when the fit is over the interval $5 \leq z \leq 14$ with $q = 0.9055$. The mass becomes smaller as additional points are discarded, however, the uncertainty rapidly grows large. If we discarded one additional point and performed the fit over the interval $6 \leq z \leq 14$, the mass estimate would be slightly smaller, but this improvement would be negated by the increased uncertainty. Therefore, we are justified in fitting over the interval $5 \leq z \leq 14$, which gives us the mass estimate $m_W = 0.4666 \pm 0.0044$.

For the Higgs mass estimate, we use the same criteria. Points $z > 10$ are discarded due to large error bars. The proposed fits are tabulated in Table (2). The goodness-of-fit is optimized, with $q = 0.9432$, if we fit over the interal $5 \leq z \leq 10$. Discarding additional points reduces the mass estimate further, but the increased uncertainty becomes too costly. Therefore, we fit over the interval $5 \leq z \leq 10$ as shown in the right panel of Fig. (1). This fit gives us the mass estimate $m_H = 0.665 \pm 0.014$.

3.4.2   1-mass Fit

As discussed in section 2.3, for sufficiently large n_t our correlation function is

$$C(n_t) \simeq A_0 e^{-m_0 n_t}.$$

The lattice has periodic boundary conditions, so the correlation functions have time translational symmetry. This leads us to a fit of the form

$$C(z) = A \left[e^{-mz} + e^{-m(N_t - z)} \right]. \tag{10}$$

The second term reflects the periodic boundary conditions and the finite time extension of the lattice. For large N_t, e.g., $N_t = 64$, it is negligible. We also exploit this symmetry to increase our statistics. The two parameters, A and m, are adjusted during the fitting process, with the mass m being the parameter of primary interest. The mass estimate is again an upper bound.

The least squares fit is a function of the error bars. So, points with smaller error bars are more heavily weighted. The actual curve-fitting process is not easily amenable

---

[1]Due to correlations between the data the goodness-of-fit loses its statistical meaning, but the fit with the largest q may still be preferred.

Proposed Fit	Included Points	q	m_W
$1 \leq z \leq 14$	14	0.0000	1.8495 ± 0.0005
$2 \leq z \leq 14$	13	0.0000	0.7337 ± 0.0011
$3 \leq z \leq 14$	12	0.0000	0.5223 ± 0.0017
$4 \leq z \leq 14$	11	0.2723	0.4763 ± 0.0028
$5 \leq z \leq 14$	10	0.9055	0.4666 ± 0.0044
$6 \leq z \leq 14$	9	0.8849	0.4630 ± 0.0071
$7 \leq z \leq 14$	8	0.8398	0.4591 ± 0.0110
$8 \leq z \leq 14$	7	0.8093	0.4693 ± 0.0186
$9 \leq z \leq 14$	6	0.8269	0.4487 ± 0.0292

Table 1: For the W correlation function plotted in the left panel of Fig. (1), we tabulate here different ratio fits. The first column gives the interval over which the fit is proposed. The second column gives the number of points included in the fit. The third column gives the goodness-of-fit q, and the final column gives the mass estimate and uncertainty from the proposed fit. The uncertainty is obtained using the jackknife method. In this example, we choose the fit $5 \leq z \leq 14$ as described in the text and displayed in the left panel of Fig. (1).

Proposed Fit	Included Points	q	m_H
$1 \leq z \leq 10$	10	0.0000	1.2199 ± 0.0009
$2 \leq z \leq 10$	9	0.0000	0.8362 ± 0.0017
$3 \leq z \leq 10$	8	0.0000	0.7244 ± 0.0035
$4 \leq z \leq 10$	7	0.6603	0.6849 ± 0.0076
$5 \leq z \leq 10$	6	0.9432	0.6649 ± 0.0140
$6 \leq z \leq 10$	5	0.8787	0.6613 ± 0.0280
$7 \leq z \leq 10$	4	0.7713	0.6498 ± 0.0511

Table 2: For the Higgs correlation function plotted in the right panel of Fig. (1), we tabulate here different ratio fits. The first column gives the interval over which the fit is proposed. The second column gives the number of points included in the fit. The third column gives the goodness-of-fit q, and the final column gives the mass estimate and uncertainty from the proposed fit. The uncertainty is obtained using the jackknife method. In this example, we choose the fit $5 \leq z \leq 10$ as described in the text and displayed in the right panel of Fig. (1).
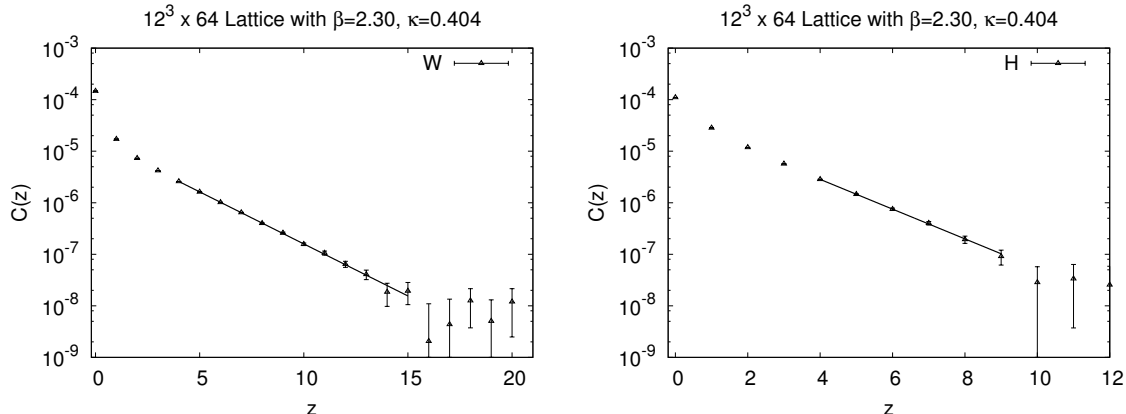
Figure 2: Here we have typical semi-log plots of $C(z)$ for the W correlation function (on the left) and the Higgs correlation function (on the right). The solid lines display the 1-mass, 2-parameter fits of the form Eq. (10) for the W mass and Higgs mass. Initial points are excluded because of unwanted higher mass contributions to the correlation function.

to automation, and manual adjustments are made after a visual examination. This is illustrated in the example fits shown in Fig. (2), where the 1-mass fit is performed for the W mass (left panel) and the Higgs mass (right panel). In this example, a $12^3 \times 64$ lattice was used, again, with $\beta = 2.30$ and $\kappa = 0.404$. The uncertainties of the mass estimates are obtained using the jackknife method.

As discussed in section 3.4.1, the time extension of the lattice used is $N_t = 64$, so $1 \leq z \leq 32$. The statistical error of the correlation functions, $C(z)$, grows large rapidly with increasing z. At the same time, $C(z)$ becomes small with increasing z. Typically, $C(z)$ becomes statistically indistinguishable from zero for z greater than some z', and we are justified in excluding $C(z > z')$ from our fits. In the example shown in Fig. (2), this occurs at $z' = 15$ for the W mass as $C(16) = (0.21 \pm 0.89) \times 10^{-8}$ is indistinguishable from zero, so we exclude $C(z > 15)$ from the fit. For the Higgs mass, this cutoff occurs at $z' = 9$ since, in this example, $C(10) = (0.29 \pm 0.29) \times 10^{-7}$ is indistinguishable from zero.

The small $z = \Delta t$ points are sensitive to high mass contributions to the correlation function. Therefore, we must neglect the lowest z values until consistency of the fit is found. There are several criteria used to determine how many initial points to exclude from the fit. The first is to optimize the goodness-of-fit q defined by Eq. (8). The second is to minimize the estimated mass. The 1-mass fit gives an upper bound, so we want to find the least upper bound.

Continuing with the same example, we examine proposed fits for the W mass in Table (3) and the Higgs mass in Table (4). For the W mass, we see that the goodness-of-fit is optimized if we fit over the interval $5 \leq z \leq 15$. The estimated mass is minimized if we fit over the interval $8 \leq z \leq 15$. Although the estimated mass decreases as more initial points are excluded, the uncertainty also grows larger.

12

Proposed Fit	Included Points	q	m_W
$0 \leq z \leq 15$	16	0.0000	2.0731 ± 0.0005
$1 \leq z \leq 15$	15	0.0000	0.6873 ± 0.0007
$2 \leq z \leq 15$	14	0.0000	0.5026 ± 0.0011
$3 \leq z \leq 15$	13	0.2452	0.4719 ± 0.0017
$4 \leq z \leq 15$	12	0.9875	0.4651 ± 0.0026
$5 \leq z \leq 15$	11	0.9891	0.4626 ± 0.0042
$6 \leq z \leq 15$	10	0.9783	0.4614 ± 0.0067
$7 \leq z \leq 15$	9	0.9631	0.4645 ± 0.0105
$8 \leq z \leq 15$	8	0.9539	0.4564 ± 0.0170
$9 \leq z \leq 15$	7	0.9348	0.4677 ± 0.0276

Table 3: For the W correlation function plotted in the left panel of Fig. (2), we tabulate here different 1-mass fits of the form Eq. (10). The first column gives the interval over which the fit is proposed. The second column gives the number of points included in the fit. The third column gives the goodness-of-fit q, and the final column gives the mass estimate and uncertainty from the proposed fit. The uncertainty is obtained using the jackknife method. In this example, we choose the fit $4 \leq z \leq 15$ as described in the text and displayed in the left panel of Fig. (2).

Proposed Fit	Included Points	q	m_H
$0 \leq z \leq 9$	10	0.0000	1.2388 ± 0.0010
$1 \leq z \leq 9$	9	0.0000	0.8134 ± 0.0019
$2 \leq z \leq 9$	8	0.0001	0.7143 ± 0.0038
$3 \leq z \leq 9$	7	0.8589	0.6805 ± 0.0074
$4 \leq z \leq 9$	6	0.9841	0.6643 ± 0.0189
$5 \leq z \leq 9$	5	0.9447	0.6637 ± 0.0281
$6 \leq z \leq 9$	4	0.8327	0.6690 ± 0.0568

Table 4: For the Higgs correlation function plotted in the right panel of Fig. (2), we tabulate here different 1-mass fits of the form Eq. (10). The first column gives the interval over which the fit is proposed. The second column gives the number of points included in the fit. The third column gives the goodness-of-fit q, and the final column gives the mass estimate and uncertainty from the proposed fit. The uncertainty is obtained using the jackknife method. In this example, we choose the fit $4 \leq z \leq 9$ as described in the text and displayed in the right panel of Fig. (2).
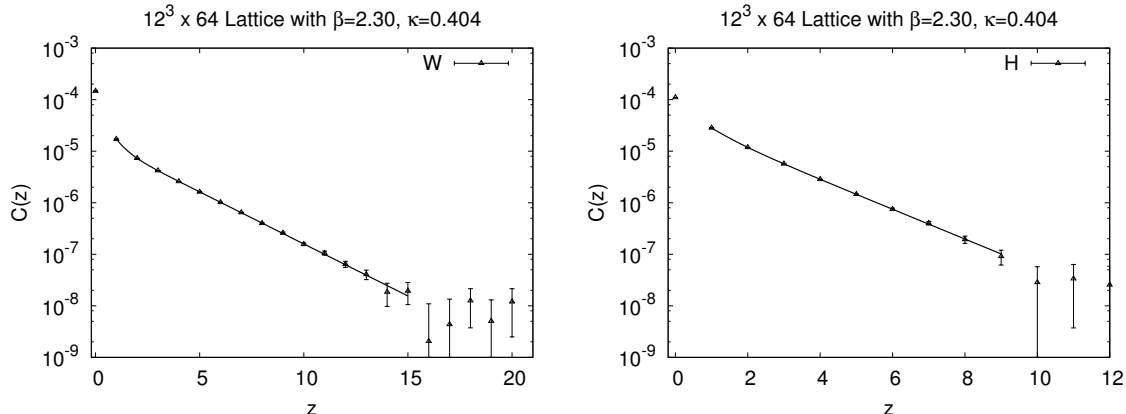
Figure 3: Here we have the same semi-log plots of $C(z)$ for the W and Higgs correlation functions. The solid lines now display the 2-mass, 4-parameter fits of the form Eq. (11) for the W-mass and Higgs mass. For the 2-mass fits, fewer initial points have to be excluded.

In this case, we choose to fit over the interval $4 \leq z \leq 15$, as shown in the left panel of Fig. (2), since excluding any additional points gains only increased uncertainty. For the Higgs mass, proposed fits are given in Table (4). The goodness-of-fit is optimized if we fit over the interval $4 \leq z \leq 9$, as shown in the right panel of Fig. (2). Excluding an additional point would give us an even lower mass estimate but also an unacceptable increase in uncertainty.

3.4.3   2-mass Fit

As discussed in Section 2.3, we also perform mass estimates by using a 2-mass, 4-parameter fit of the form

$$C(n_t) \simeq A_0 e^{-m_0 n_t} + A_1 e^{-m_1 n_t}.$$

In practice, to account for the finite time extension and periodic boundary conditions, we fit to

$$C(z) = A_1 \left[e^{-mz} + e^{-m(N_t - z)} \right] + A_2 \left[e^{-m'z} + e^{-m'(N_t - z)} \right], \qquad (11)$$

where our parameter of primary interest is the smaller mass m. This mass estimate is no longer an upper bound.

As with the 1-mass fit, we again use the Levenberg-Marquardt least squares fit. Again, the error bars are computed via jackknife resampling, and now we correct for bias in the estimator by performing a second level jackknife resampling. When choosing the best fit, we again look at the goodness-of-fit defined by Eq. (8). We also compare the 2-mass fit with the 1-mass fit, checking that the 2-mass fit is within the margin of error of the 1-mass fit. Examples of 2-mass fits are shown in Fig. (3). These are from the same $12^3 \times 64$ simulation with $\beta = 2.30$ and $\kappa = 0.404$ as used in previous examples.

Proposed Fit	Included Points	q	m_W
$0 \leq z \leq 15$	16	0.000	0.4873 ± 0.0037
$1 \leq z \leq 15$	15	0.993	0.4651 ± 0.0029
$2 \leq z \leq 15$	14	0.991	0.4633 ± 0.005
$3 \leq z \leq 15$	13	0.991	0.47 ± 0.13

Table 5: For the W correlation function plotted in the left panel of Fig. (3), we tabulate here different 2-mass fits of the form Eq. (11). The first column gives the interval over which the fit is proposed. The second column gives the number of points included in the fit. The third column gives the goodness-of-fit q, and the final column gives the mass estimate and uncertainty from the proposed fit. These estimates are bias corrected using the jackknife method, and the uncertainty is obtained from a second level jackknife resampling. In this example, we choose the fit $1 \leq z \leq 15$ as described in the text and displayed in the left panel of Fig. (3).

Proposed Fit	Included Points	q	m_H
$0 \leq z \leq 9$	10	0.28	0.6894 ± 0.0093
$1 \leq z \leq 9$	9	0.988	0.666 ± 0.019
$2 \leq z \leq 9$	8	0.944	0.67 ± 0.31
$3 \leq z \leq 9$	7	0.952	0.665 ± 0.083

Table 6: For the Higgs correlation function plotted in the right panel of Fig. (3), we tabulate here different 2-mass fits of the form Eq. (11). The first column gives the interval over which the fit is proposed. The second column gives the number of points included in the fit. The third column gives the goodness-of-fit q, and the final column gives the mass estimate and uncertainty from the proposed fit. These estimates are bias corrected using the jackknife method, and the uncertainty is obtained from a second level jackknife resampling. In this example, we choose the fit $1 \leq z \leq 9$ as described in the text and displayed in the right panel of Fig. (3).

We again exclude $C(z > 15)$ from the fit for the W mass and $C(z > 9)$ from the fit for the Higgs mass, like we did for the 1-mass fits and for the same reason. For the 2-mass fits, fewer initial points have to be excluded. Again, we look at the goodness-of-fit to determine whether to exclude an initial point. Proposed fits are given in Table (5) for the W mass and in Table (6) for the Higgs mass. For the W mass, we see that the goodness-of-fit is optimized if we fit over the interval $1 \leq z \leq 15$, as shown in the left panel of Fig. (3). For the Higgs mass, the goodness-of-fit is optimized if we fit over the interval $1 \leq z \leq 9$, as shown in the right panel of Fig. (3).

3.4.4 Comparing Estimators

We have described three different mass estimators: the ratio fit, the 1-mass fit, and the 2-mass fit. How do they compare, and what are the benefits and drawbacks of each?

For the ratio fit, we know that for large z,

$$m_0 \simeq \ln \left[\frac{C(z)}{C(z+1)} \right].$$

Here, the estimate is an upper bound. Ideally, one could get a best estimate of m_0 simply by plugging the two points with largest z into this formula. However, as detailed earlier, large z brings along large statistical error in $C(z)$. Fortunately, the logarithm of the ratio decays quickly to near the asymptotic value before the statistical errors grow too large. Thus, one can get an estimate of m_0 by examining the middle values. A simple estimate of m_0 is obtained by selecting the point with the least upper error bar. A better method, and the one we used here, is to exclude initial points and fit a horizontal line to the remaining points as illustrated in Fig. (1). The criteria for excluding an initial point, described in Section 3.4.1, include maximizing the goodness-of-fit given by Eq. (8) and minimizing the mass estimate.

For the 1-mass fit, we fit $C(z)$ to a function of the form

$$Ae^{-m_0 z},$$

to estimate m_0. The estimate is again an upper bound. Because our fit neglects the contribution of higher energy states, we typically have to exclude the first points. It is only for large z that the lowest energy state dominates. On the other hand, $C(z)$ has large uncertainty for large z. The error and an estimate of the bias is calculated using a jackknife approach. Mostly, the bias is small for the 1-mass fits, so no bias correction is made.

For the 2-mass fit, we fit $C(z)$ to a function of the form

$$A_0 e^{-m_0 z} + A_1 e^{-m_1 z}, \qquad m_1 > m_0,$$

to estimate m_0. Now the estimate is no longer an upper bound. In principle, this is a more reliable estimator because it includes the second exponential term. With the 2-mass fit, fewer initial points have to be excluded from the fit. For large z, the same statistical error occurs as with the 1-mass and ratio fits. Again, the error and an estimate of the bias is calculated using a jackknife approach. With the 2-mass fit, the bias is too large to ignore, so a bias corrected estimator is used. The statistical error of these estimates is calculated using a second level jackknife analysis.

The downside of all three estimators is that a lot of time is spent checking the quality of fits and manually adjusting them. These manual adjustments are unavoidable particularly for the 1-mass and 2-mass estimators, which cannot be automated in a straightforward manner. If time is an issue or if there is too much data to analyze manually, the ratio fit seems the most attractive estimator. As discussed in Section 3.4.1, points $z > z'$, where z' is the smallest z for which $C(z)/C(z+1) < 1$, are automatically discarded. In our case, with $12^3 \times 64$ lattices, an automated fit over the interval $\lfloor z'/2 \rfloor \leq z \leq z'$ provided quick and reasonably precise results. However, for

the most precise results, the choice of fitting interval depends on the goodness-of-fit and the magnitude of the mass estimate as described in Section 3.4.1.

To get a sense of the consistency between the three estimators, we compare the mass estimates from all three estimators for a number of data points. Ten simulations were performed on $12^3 \times 64$ lattices, with $\beta = 2.30$, and $0.401 \leq \kappa \leq 0.411$ (Run times are discussed in Section 4). For the ratio and 1-mass fits, the error bars were obtained via the jackknife method. For the 2-mass fit, the estimate was first bias corrected via the jackknife method, and the error bar was obtained via a second level jackknife analysis.

The results for the W mass are tabulated in Table (7) and displayed in Fig. (4). For any given κ, we see that the three different estimators tend to be within error bars of each other. Even when they are not, the difference does not appear to be statistically significant. For a more objective appraisal, we use the Gaussian difference test discussed in Section 3.1. The results are given in the last three columns of Table (7). For example, to compare $m_W = 0.4670 \pm 0.0076$ from the ratio fit and $m_W = 0.4696 \pm 0.0033$ from the 1-mass fit, we compute Q defined in Eq. (6). For this example, we find that $Q = 0.75$. We compare all of the mass estimates in this manner. Column Q_{R1} compares the ratio fit and 1-mass fit estimates, column Q_{R2} compares the ratio fit and 2-mass fit estimates, and column Q_{12} compares the 1-mass fit and 2-mass fit estimates. We find that $Q \geq 0.05$ for all of these, so we conclude that the systematic error, due to different fitting procedures, is smaller than a reasonable statistical error. We also see that the error bars on the estimates from the ratio fit tend to be larger than for the other two estimators, so at least for the W mass, we get more precise results by using the 1-mass or 2-mass estimator.

The results for the Higgs mass are tabulated in Table (8) and displayed in Fig. (5). For any given κ, we again see that the three different estimators tend to be within error bars of each other. For a more objective appraisal, we again use the Gaussian difference test discussed in Section 3.1. The results are given in the last three columns of Table (8). Column Q_{R1} compares the ratio fit and 1-mass fit estimates, column Q_{R2} compares the ratio fit and 2-mass fit estimates, and column Q_{12} compares the 1-mass fit and 2-mass fit estimates. We find that $Q \geq 0.05$ for all of these, so we conclude that our three estimators are also consistent for the Higgs mass. For the Higgs mass, we see that the error bars on the estimates from the ratio fit tend to be smaller than for the other two estimators. So, for the Higgs mass, we get more precise results by using the ratio fit. This occurs because m_H is larger than m_W, so there is faster falloff for the correlation function.

These comparisons show that there is good consistency between the three different estimation methods. There is not always a clear reason to prefer one estimator over another, yet they are not redundant. Having three different but consistent estimators at one's disposal gives a double and triple-check on mass estimates. Furthermore, in specific cases, one estimator may outperform the others. In the comparison of the W-mass estimates given above, the ratio fit had larger error bars, suggesting

	Ratio Fit		1-mass Fit		2-mass Fit		Gaussian Differences		
κ	m_W	Δm_W	m_W	Δm_W	m_W	Δm_W	Q_{R1}	Q_{R2}	Q_{12}
0.401	0.4670	0.0076	0.4696	0.0033	0.4608	0.0041	0.75	0.47	0.09
0.402	0.4471	0.0110	0.4666	0.0052	0.4676	0.0043	0.11	0.08	0.88
0.403	0.4647	0.0047	0.4656	0.0032	0.4672	0.0036	0.87	0.67	0.74
0.404	0.4666	0.0044	0.4651	0.0035	0.4651	0.0029	0.79	0.78	1.00
0.405	0.4612	0.0065	0.4694	0.0040	0.4698	0.0031	0.28	0.23	0.94
0.406	0.4552	0.0088	0.4604	0.0038	0.4544	0.0064	0.59	0.94	0.42
0.407	0.4537	0.0088	0.4595	0.0054	0.4581	0.0072	0.57	0.70	0.88
0.408	0.4694	0.0062	0.4685	0.0046	0.4752	0.0026	0.91	0.39	0.20
0.410	0.4797	0.0033	0.4798	0.0029	0.4784	0.0026	0.98	0.76	0.72
0.411	0.4516	0.0134	0.4696	0.0038	0.4584	0.0091	0.20	0.67	0.26

Table 7: Here we compare the three fits by estimating the W-mass, m_W, at various values of κ. Each was performed on a $12^3 \times 64$ lattice with $\beta = 2.30$. The first column gives the value of κ, the next two give the mass estimate and statistical error of the ratio fit estimator, the next two give the mass estimate and error of the 1-mass fit estimator, and the next two give the mass estimate and error of the 2-mass fit estimator. The last three columns give the Gaussian differences between the estimates. Column Q_{R1} compares the ratio fit and 1-mass fit estimates, column Q_{R2} compares the ratio fit and 2-mass fit estimates, and column Q_{12} compares the 1-mass fit and 2-mass fit estimates.
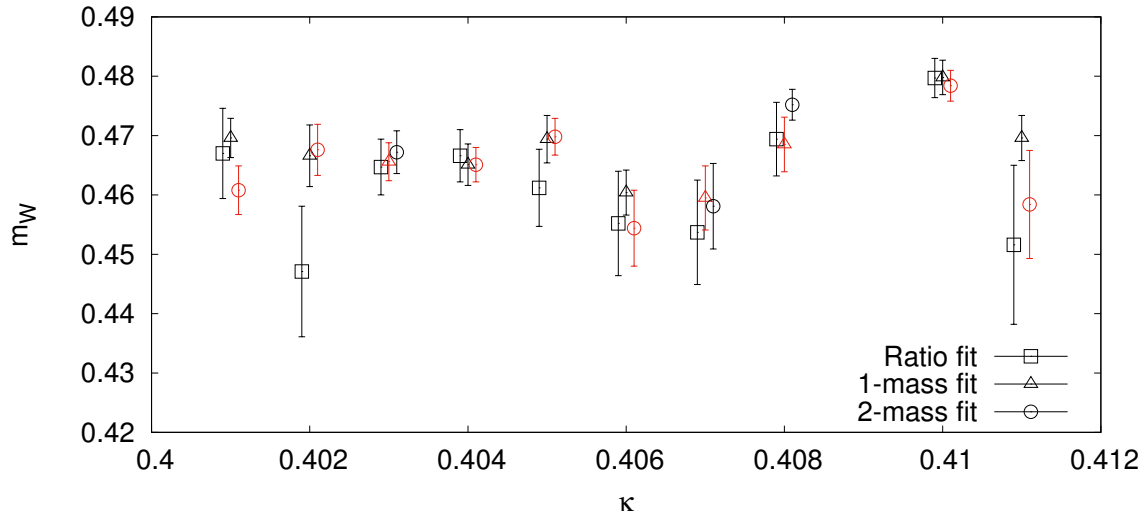
Figure 4: A plot of the W mass, m_W, versus κ. Each was performed on a $12^3 \times 64$ lattice with $\beta = 2.30$. The results of each of the three estimators are plotted for comparison with each other. For any given κ, the three different estimators tend to agree within error bars. Note: For example, the first three points are all at $\kappa = 0.401$. They are slightly displaced from each other so their error bars can be differentiated. The best estimate, taking into consideration the magnitude of the mass estimate and its uncertainty, is highlighted in red.

	Ratio Fit		1-mass Fit		2-mass Fit		Gaussian Differences		
κ	m_H	Δm_H	m_H	Δm_H	m_H	Δm_H	Q_{R1}	Q_{R2}	Q_{12}
0.401	0.513	0.020	0.532	0.020	0.528	0.024	0.50	0.63	0.90
0.402	0.589	0.015	0.586	0.021	0.579	0.026	0.91	0.74	0.83
0.403	0.590	0.020	0.618	0.018	0.617	0.027	0.30	0.42	0.98
0.404	0.665	0.014	0.664	0.019	0.666	0.019	0.97	0.97	0.94
0.405	0.695	0.017	0.691	0.025	0.691	0.031	0.89	0.91	1.00
0.406	0.756	0.013	0.756	0.020	0.754	0.028	1.00	0.95	0.95
0.407	0.777	0.011	0.748	0.026	0.752	0.031	0.30	0.45	0.92
0.408	0.800	0.010	0.796	0.014	0.8083	0.009	0.82	0.54	0.46
0.410	0.833	0.013	0.830	0.016	0.803	0.036	0.88	0.43	0.49
0.411	0.878	0.020	0.905	0.012	0.882	0.016	0.25	0.88	0.25

Table 8: Here we compare the three fits by estimating the Higgs-mass, m_H, at various values of κ. Each was performed on a $12^3 \times 64$ lattice with $\beta = 2.30$. The first column gives the value of κ, the next two give the mass estimate and statistical error of the ratio fit estimator, the next two give the mass estimate and error of the 1-mass fit estimator, and the next two give the mass estimate and error of the 2-mass fit estimator. The last three columns give the Gaussian differences between the estimates. Column Q_{R1} compares the ratio fit and 1-mass fit estimates, column Q_{R2} compares the ratio fit and 2-mass fit estimates, and column Q_{12} compares the 1-mass fit and 2-mass fit estimates.
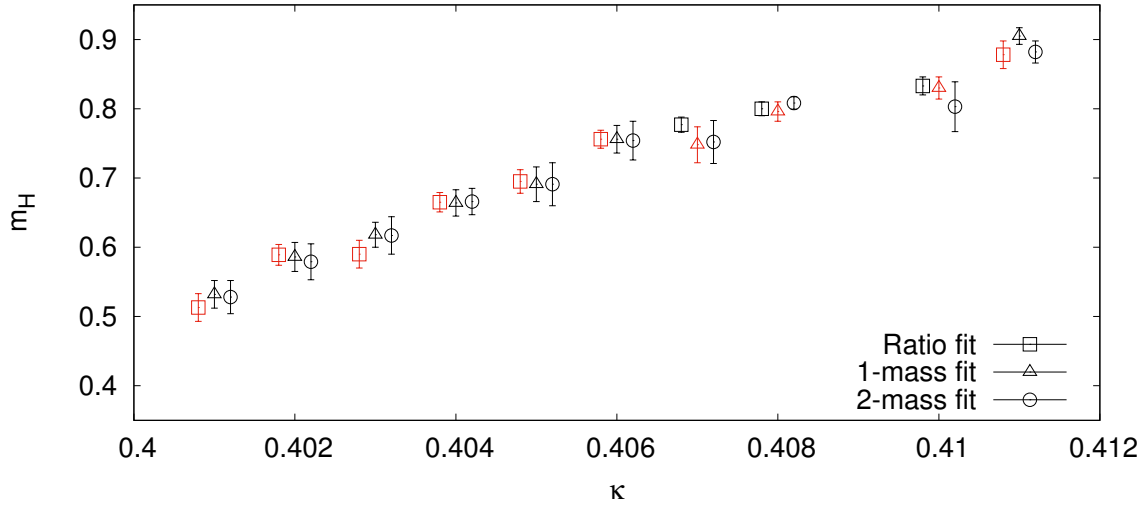
Figure 5: A plot of the Higgs-mass m_H versus κ. Each was performed on a $12^3 \times 64$ lattice with $\beta = 2.30$. The results of each of the three estimators are plotted for comparison with each other. For any given κ, the three different estimators tend to agree to within error bars. Note: For example, the first three points are all at $\kappa = 0.401$. They are slightly displaced from each other so their error bars can be differentiated. The best estimate, taking into consideration the magnitude of the mass estimate and its uncertainty, is highlighted in red.

better results if one of the other two estimators is used. However, for the Higgs mass estimates, the opposite was true. The ratio fit tended to give the smallest error bars, making it the more attractive estimator for those masses.

4   Application of Mass Estimates

A principal goal of the larger LGT project at FSU is to search for numerical evidence in favor or against a pseudo continuum limit $[m\,a(\beta)] \to 0$ with the mass ratio $m_H/m_W = 1.6$ held constant near the known [1] experimental value. MCMC simulations are used to obtain correlation functions and then various mass estimators can be used to numerically estimate the Higgs and W masses, m_H and m_W. In my project, the investigation is limited to the $\lambda \to \infty$ limit. Exploring the full parameter space was not possible in the time at our disposal.

Each data point was obtained from an MCMC Fortran simulation. These simulations are resource intensive, but the run time is reduced by parallelization employing Message Passing Interface (MPI). Even so, a relatively small $8^3 \times 64$ simulation with 2^{16} equilibrating sweeps followed by 64 bins of 2^{10} measurements with 16 sweeps between measurements takes about a week running on eight processors. To reduce the error bars in our results, we often ran simulations that took several times longer. When statistical uncertainty necessitated it, we ran much larger simulations at the National Energy Research Scientific Computing Center (NERSC).

From each MCMC simulation, we can estimate the mass ratio m_H/m_W for the given value of β and κ by applying one or more of the mass estimators. Recall that β is inversely proportional to the bare coupling constant g. When, as in pure SU(2) LGT, the lattice spacing a decreases with decreasing g, the limit $\beta \to \infty$ is equivalent to the pseudo continuum limit $a\,m_W \to 0$. If $a\,m_W$ approaches a nonzero value when $\beta \to \infty$, then the continuum limit does not exist. This would suggest a first order phase transition at that energy scale and could be a signal for new physics.

The mass ratio estimates depend not only on β but also on the hopping parameter κ. For a given lattice size (e.g. $12^3 \times 64$), we choose a β value. Then we run a number of MCMC simulations at different κ values. Each simulation gives us a mass ratio estimate m_H/m_W, so after running a number of simulations with fixed β, we can plot the mass ratio versus κ. Assuming that the mass ratio as a function of κ is continuous and smooth, we can apply a linear fit in a neighborhood of $m_H/m_W = 1.6$, as shown in Fig. (6). Where this linear fit intersects the horizontal line $m_H/m_W = 1.6$, we find the actual value of κ for that value of β. By repeating this process for different values of β, we obtain a relation between β and κ for a given lattice size. In Fig. (6), the mass ratio is plotted versus κ for β ranging from 2.3 to 2.8. Those simulations were performed on lattices of size $12^3 \times 64$. Running additional simulations on larger lattices (e.g., $16^3 \times 64$ and $20^3 \times 64$ lattices) is necessary to estimate finite lattice size corrections.

A plot of the mass ratio estimates m_H/m_W versus $a\,m_W$ is shown in Fig. (7). Each
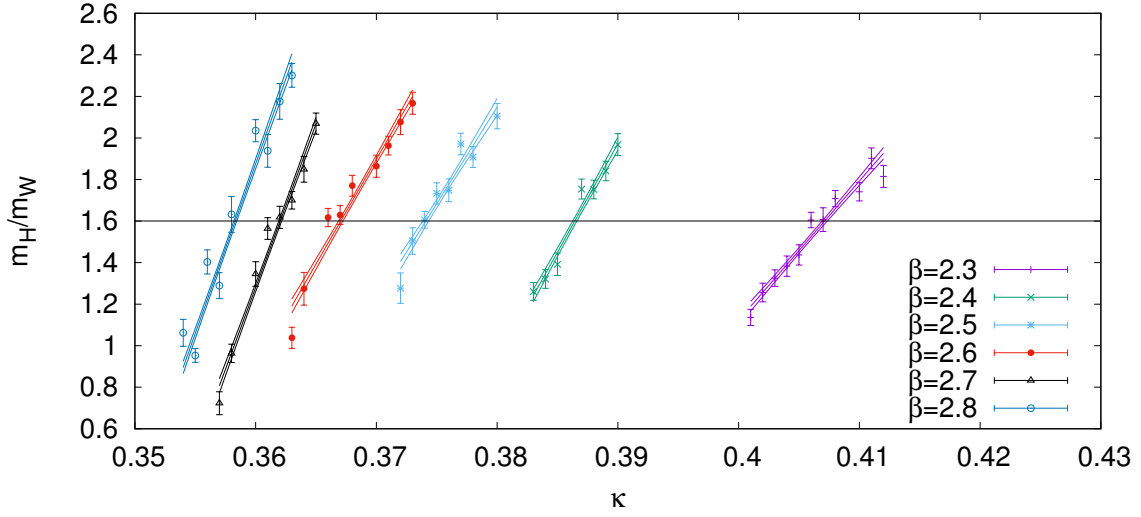
Figure 6: A plot of the mass ratio m_H/m_W (vertical axis) versus κ (horizontal axis) for different values of β. The horizontal line at $m_H/m_W = 1.6$ is the known value of the mass ratio. Each point is the output of an MCMC simulation on a $12^3 \times 64$ lattice. The 1-mass estimator was used to estimate the masses.
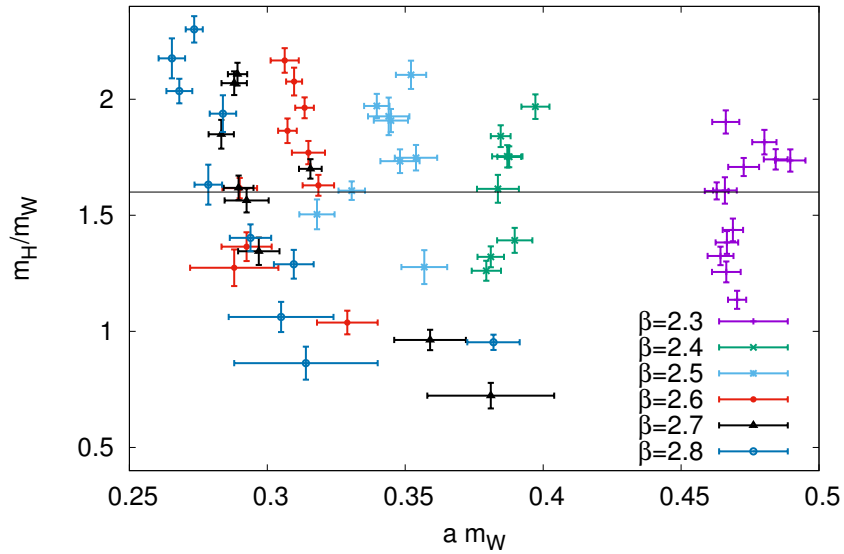
Figure 7: In this figure, the mass ratios are plotted versus the W-mass for a range of β values. Each colored cluster is a set of mass ratio estimates with various κ and a fixed β. The 1-mass estimator was used to estimate the masses.

21

cluster in this figure is a set of mass ratio estimates with various κ and a fixed β. The value of β for each cluster is noted in the legend. Recall the pseudo continuum limit $a\,m_W \to 0$ as $\beta \to \infty$. This plot shows an obvious decrease in $a\,m_W$ when β goes from 2.3 to 2.4. As β increases beyond that, $a\,m_W$ decreases further, but the data becomes noisy. This plot suggests that $a\,m_W$ may converge to a positive value near 0.25, that is, there may be no continuum limit. Further investigation is necessary before we can report evidence for or against the limit $a\,m_W \to 0$. In particular, simulations must be performed at larger values of β, and finite lattice size corrections must be controlled. For this purpose, the statistical noise must be reduced by performing larger simulations.

5 Summary and Conclusions

In quantum field theory (QFT), the physics is contained in infinite-dimensional path integrals. In lattice gauge theory (LGT), the four-dimensional Minkowski spacetime of QFT becomes a four-dimensional Euclidean spacetime on a finite, discrete lattice with lattice sites separated by distance a. Masses can now be extracted from correlation functions of the form

$$C(n_t) = \sum_k \langle 0|\hat{O}|k\rangle \, \langle k|\hat{O}^\dagger|0\rangle \, e^{-n_t E_k} = A_0 e^{-m_0 n_t} + A_1 e^{-m_1 n_t} + \cdots.$$

The quantum continuum limit is obtained by driving the couplings of the theory to their critical values. In this thesis, I performed Markov Chain Monte Carlo (MCMC) simulations for the SU(2) Higgs model and looked at the pseudo continuum limit $m\,a \to 0$.

The correlation functions can be computed using MCMC simulations. Then particle masses can be estimated from the exponential falloff of those correlation functions using a number of different estimators. Mass estimates have several important uses in LGT. For example, mass ratios can be used to investigate the existence of a continuum limit. Such an investigation could reveal a phase transition that would imply new physics at some scale.

In this thesis, I discussed three different mass estimators. Taking the natural logarithm of the ratio of consecutive correlation functions gives us the "ratio fit" estimator

$$m(z) = \ln\left(\frac{C(z)}{C(z+1)}\right) \to m_0.$$

The function $m(z)$ approaches the mass of interest, m_0, in the large z limit. This function decays quickly to the asymptotic limit, but the statistical error also grows quickly. A suitable estimate of m_0 is obtained by discarding the first points of $m(z)$ and fitting a horizontal line to the remaining points. The "1-mass fit" is obtained by fitting the correlation function $C(z)$ to an exponential function

$$C(z) \simeq A e^{-mz},$$

22

to estimate $m_0 \simeq m$. This fit neglects the contribution of higher energy states, so we typically have to exclude the first points. It is only for large z that the lowest energy state dominates. The "2-mass fit" is obtained by fitting $C(z)$ to a function of the form

$$C(z) \simeq A_0 e^{-mz} + A_1 e^{-m_1 z},$$

to estimate $m_0 \simeq m$. With the 2-mass fit, fewer initial points have to be excluded. For large z, the same statistical error occurs as with the 1-mass and ratio fits. The error of each estimator is calculated using a jackknife approach and the bias is estimated. For the ratio and 1-mass fits, no bias correction is made. For the 2-mass fit, the bias is too large to ignore, so a bias corrected estimator is used. The statistical error is then calculated using a second level jackknife analysis.

In this thesis, using data from ten simulations performed on $12^3 \times 64$ lattices, I compared the three mass estimators and showed that they are consistent. With each estimator, I estimated the Higgs and W boson masses for each of the ten runs. Although they performed similarly, each estimator exhibited different qualities. I found that in specific cases, one may outperform the other two. For the W mass, I found that the 1-mass and 2-mass estimators were marginally more precise. For the Higgs mass, I found the opposite to be true. The ratio fit was more precise than either the 1-mass or 2-mass estimator. Even if one doesn't need a triple check, having three consistent mass estimators gives one a choice in selecting the best one for the task.

References

[1] G. Aad et al. (ATLAS and CMS Collaboration), "Combined measurement of the Higgs boson mass in pp collisions at $\sqrt{s} = 7$ and 8 TeV with the ATLAS and CMS experiments," Phys. Rev. Lett. **114**, 191803 (2015).

[2] M. Aizenman, "Proof of the triviality of ϕ_d^4 field theory and some mean field features of Ising models for $d > 4$," Phys. Rev. Lett. **47**, 1 (1981).

[3] B. Berg, *Markov Chain Monte Carlo Simulations and Their Statistical Analysis* (World Scientific, 2004).

[4] C. Gattringer and C. B. Lang, *Quantum Chromodynamics on the Lattice* (Springer, 2010).

[5] U. Heller, "Status of the Higgs mass upper bound," Nucl. Phys. B (Proc. Suppl.) **34**, 101 (1994).

[6] W. Langguth, I. Montvay, and P. Weisz, "Monte carlo study of the standard SU(2) Higgs model," Nucl. Phys. B **277**, 11 (1986).

[7] K. Levenberg, "A Method for the Solution of Certain Non-Linear Problems in Least Squares," Quarterly of Applied Mathematics. **2**, 164 (1944).

[8] D. Marquardt, "An Algorithm for Least-Squares Estimation of Nonlinear Parameters," SIAM Journal on Applied Mathematics. **11** (2) 431 (1963).

[9] I. Montvay and G. Münster, *Quantum Fields on a Lattice* (Cambridge UP, 1994).

[10] K. Osterwalder and R. Schrader, "Axioms for Euclidean Green's Functions," Comm. Math. Phys. **31**, 83 (1973); **42**, 281 (1975).

[11] W. H. Press et al, *Numerical Recipes in C: The Art of Scientific Computing*, Ed. 2 (Cambridge, 1992), pp. 216-221.

[12] O. J. Rosten, "Triviality from the Exact Renormalization Group," JHEP **0907**, 019 (2009) [arXiv: 0808.0082], and references therein.

[13] J. Smit, *Cambridge Lecture Notes in Physics : Introduction to Quantum Fields on a Lattice* (Cambridge University Press, 2002).

[14] K. Wilson, "Confinement of Quarks," Phys. Rev. D **10**, 2445 (1974).

[15] K. Wilson and J. Kogut, "The renormalization group and the ϵ expansion", Phys. Lett. C **12**, 75 (1974).

[16] U. Wolff, "Precision check on triviality of ϕ^4 theory by a new simulation method," Phys. Rev. D **79**, 105002 (2009), and references therein.